Journal of
Materials Chemistry A

Materials for energy and sustainability

## Accepted Manuscript

This article can be cited before page numbers have been issued, to do this please use: B. N. Bhadra, R. N. Acharyya, S. Shahi, K. Ariga and L. K. Shrestha, *J. Mater. Chem. A*, 2026, DOI: 10.1039/D6TA01685E.


This is an Accepted Manuscript, which has been through the Royal Society of Chemistry peer review process and has been accepted for publication.

Accepted Manuscripts are published online shortly after acceptance, before technical editing, formatting and proof reading. Using this free service, authors can make their results available to the community, in citable form, before we publish the edited article. We will replace this Accepted Manuscript with the edited and formatted Advance Article as soon as it is available.

You can find more information about Accepted Manuscripts in the Information for Authors.

Please note that technical editing may introduce minor changes to the text and/or graphics, which may alter content. The journal's standard Terms & Conditions and the Ethical guidelines still apply. In no event shall the Royal Society of Chemistry be held responsible for any errors or omissions in this Accepted Manuscript or any consequences arising from the use of any information it contains.

ROYAL SOCIETY OF CHEMISTRY

rsc.li/materials-a

View Article Online
DOI: 10.1039/D6TA01685E

ARTICLE

# Metal-Organic Framework on Fullerene (MOFOF) Derived Co-anchored Hierarchical Carbon Nanocomposite for Catalytic Nitroarene Reduction

Received 00th January 20xx,
Accepted 00th January 20xx

DOI: 10.1039/x0xx00000x

Biswa Nath Bhadra,*[ab] Rabindra Nath Acharyya,[ac#] Sabina Shahi,[ac#] Katsuhiko Ariga*[ad] and Lok Kumar Shrestha *[ae]

The catalytic reduction of nitroarenes to anilines is vital in industrial and environmental chemistry for the production of pharmaceuticals, dyes, agrochemicals, and polymers. However, traditional catalysts often struggle with issues related to activity, stability, and reusability. This study introduces a novel method for synthesizing a Co-anchored hierarchical carbon nanocomposite derived from a newly architected metal-organic framework (MOF) on fullerene (MOFOF) composite. The method involves in-situ growth of MOF (ZIF-67) on a surface-modified self-assembled fullerene nanotube ($FNT_{ox}$) with varying $Co^{2+}/C_{60}$ ratios (0.5, 1.0, 1.5, and 2.0), followed by pyrolysis under a nitrogen atmosphere. The resulting nanohybrids, particularly Co@HC-1.0 derived from MOFOF-1.0 with a $Co^{2+}/C_{60}$ ratio of 1.0, demonstrated exceptional catalytic performance for nitroarene reduction, exhibiting high activity and reusability. Characterization techniques, including SEM, XRD, Raman spectroscopy, and nitrogen sorption isotherms, confirmed the structural and morphological stability of the composites. The Co@HC-1.0 catalyst demonstrated superior, highly competitive catalytic performance, achieving a reaction rate constant of $9.25\times10^{-1}$ $min^{-1}$ and a TOF of 486 $h^{-1}$, with significant retention of performance across multiple cycles, highlighting its potential for various synthetic applications.

## 1. Introduction

Studies have confirmed that nitroarenes are highly detrimental to human health and the environment, and thus have been designated a priority contaminant by the Agency of Environmental Protection.[1–4] These toxic nitroarenes or nitrophenols can be readily converted to aromatic amines/phenols via catalytic reduction.[4–7] Consequently, catalytic reduction of nitroarenes to anilines is critical for both environmental and industrial concerns, playing a pivotal role in the synthesis of pharmaceuticals, dyes, agrochemicals, and polymers.[8–10] However, traditional catalysts often encounter limitations in activity, stability, and reusability, necessitating the development of advanced catalytic materials to overcome these challenges. In this context, carbon-based nanocomposites have attracted significant attention due to their high surface area, excellent thermal stability, and tunable porosity.

Cobalt (Co) is a transition metal known for its excellent catalytic activity and ability to facilitate various redox reactions, especially when incorporated into an appropriate support material.[11–14] Cobalt supported on a carbon matrix can enhance the catalyst's overall performance by providing active sites for catalytic reactions and improving the material's electronic conductivity. The synergy between cobalt and carbon materials yields highly efficient and durable catalysts. The fabrication of Co-doped carbon nanocomposites involves several critical steps to ensure uniform dispersion of cobalt nanoparticles within the carbon matrix and to develop a hierarchical structure that maximizes catalytic efficiency. Design and synthesis of an ideal carbon-cobalt precursor composition is one of the most critical steps toward obtaining a cobalt-anchored hierarchical carbon nanocomposite with outstanding catalytic properties.

Metal-organic frameworks (MOFs) are interesting materials with unique properties, and their combination with various materials has shown promise across many fields.[15–25] In addition, MOFs and their composites are used as precursors to produce functional carbon materials with significant potential for applications in energy storage, catalysis, and environmental remediation.[26–34] To date, cobalt-based MOFs or MOF composites have shown promise for producing fascinating

[a.] Research Center for Materials Nanoarchitectonics (MANA), National Institute for Materials Science (NIMS), 1-1 Namiki, Tsukuba, Ibaraki 305-0044, Japan. Email: bbhadra1981@gmail; ARIGA.Katsuhiko@nims.go.jp; SHRESTHA.Lokkumar@nims.go.jp
[b.] Institute Charles Gerhardt Montpellier (ICGM), Centre national de la recherche scientifique (CNRS), Montpellier, 34095, France
[c.] Graduate School of Science and Technology, University of Tsukuba, 1-1-1 Tennodai, Tsukuba, Ibaraki 305-8573, Japan
[d.] Department of Advanced Materials Science, Graduate School of Frontier Sciences, The University of Tokyo, 5-1-5 Kashiwanoha, Kashiwa, Chiba 277-8561, Japan
[e.] Department of Materials Science, Institute of Pure and Applied Sciences, University of Tsukuba, 1-1-1 Tennodai, Tsukuba, Ibaraki 305-8573, Japan
# These authors contributed equally

Supplementary Information available: [Additional TEM images; XRD and Raman data, nitrogen adsorption isotherms and the corresponding pore size distribution profiles]. See DOI: 10.1039/x0xx00000x

metallic cobalt-anchored carbons.[35–40] However, ongoing research focuses on engineering new precursor compositions to create metallic cobalt-anchored hybrid carbons with highly fascinating physicochemical features, including porosity and dispersion, leading to enhanced catalytic and fascinating electrochemical and magnetic properties, even with low cobalt loading. For example, ZIF-67 (a typical cobalt MOF) and its composites were found to be effective precursors for cobalt-decorated carbon nanocomposites used in various catalytic reactions.[36–40] Besides, fullerene nanostructures can be transformed into unique carbonaceous materials featuring porous architectures enriched in defective and graphitic walls through the removal of organic components and structural rearrangement during high-temperature treatment.[41–46] Therefore, combining the advantages of ZIF-67 and fullerenes into a composite material offers strong potential for producing advanced carbon nanomaterials with unique properties and functionalities after high-temperature carbonization.

Owing to the complementary physicochemical properties of fullerene and ZIF-67, the resulting material represents the first example of a Co-anchored nanohybrid supported on two distinct carbon matrices. Consequently, the composite exhibits superior catalytic activity and selectivity compared to existing catalysts, underscoring its strong potential for diverse synthetic and catalytic applications.

This paper presents a novel method for synthesizing a carbon nanocomposite derived from MOFOF, followed by an investigation of its catalytic performance in the reduction of nitroarenes and thorough material characterization. Unlike conventional ZIF-67-derived carbons, the present MOFOF approach uniquely integrates fullerene nanotubes as a secondary carbon scaffold, resulting in a dual-carbon hierarchical framework. This distinctive architecture enables improved dispersion of Co nanoparticles, controlled particle size, and enhanced electronic interactions among Co, N-doped carbon, and graphitic domains, features that are not attainable in traditional single-precursor MOF-derived carbons. Due to the fascinating structure and physicochemical properties of fullerene and MOF (ZIF-67), the resulting carbon composite represents the first example of a Co-anchored nanohybrid supported on two distinct carbon matrices. Consequently, the composite exhibits superior catalytic activity and selectivity compared to existing catalysts, underscoring its strong potential for diverse synthetic and catalytic applications.

## 2. Experimental

### 2.1 Materials and Methods

The materials used in this study were sourced from commercial suppliers and used without additional purification. The supporting information comprehensively covers the materials list, FNT synthesis methodology, surface modification techniques, carbonization procedures, characterization methods, and the protocol for conducting catalytic tests.

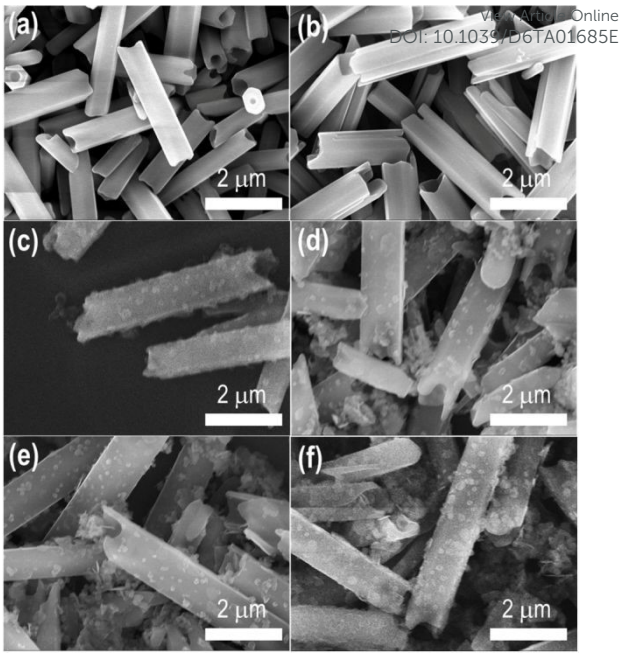


**Fig. 1**. SEM images of (a) FNT, (b) $FNT_{ox}$, (c) MOFOF-0.5, (d) MOFOF-1.0, (e) MOFOF-1.5 and (f) MOFOF-2.0.

## 3. Results and discussion

### 3.1 Synthesis and structural characterizations

Fig. 1 illustrates the scanning electron micrographs (SEM) of the FNT, acid-treated FNT ($FNT_{ox}$), and MOFOFs with four different compositions. The SEM images (Fig. 1a and Fig. 1b) of FNT and $FNT_{ox}$ show the morphological stability of FNT under ultrasonic treatment in a strong acid mixture of $HNO_3/H_2SO_4$ (1/1). The morphology of the $FNT_{ox}$ remained unchanged, with a slight destruction of some particles even after the successful decoration of the ZIF-67 onto the surface of the $FNT_{ox}$. Fig. 1c-f, the SEM images, depict almost perfect growth of the ZIF-67 particles with uniform distribution onto the $FNT_{ox}$, indicating successful assembly of ZIF-67-on-FNT composites with different ZIF-67 and fullerene ratios. As expected, the density of ZIF-67 particles can be well controlled; for example, it increased with increasing the ZIF-67 precursor ratio. The TEM images (Fig. S1) of the selected MOFOF-1.0 confirmed the perfect incorporation of the ZIF-67 particles both into the hole and surface of the $FNT_{ox}$.

The dried $FNT_{ox}$, pZIF-67, MOFOF-0.5, MOFOF-1.0, MOFOF-1.5, and MOFOF-2.0 materials underwent pyrolysis at 800 °C for 4 hours under $N_2$ flow. Subsequently, the resultant materials (excluding $FNT_{ox}$-derived carbon (FDC)) underwent HF etching (0.2 M) at 60 °C for 12 hours to eliminate soluble impurities (e.g., isolated Co species). This process yielded Co@HC-0.5, Co@HC-1.0, Co@HC-1.5, and Co@HC-2.0 carbon nanohybrids with a consistent gross yield of 22-25 wt% of the precursor materials. Conversely, Co@ZDC exhibited a yield of approximately 15 wt% after the HF washing.

Fig. 2a presents the XRD patterns of $FNT_{ox}$, ZIF-67, and MOFOF-1.0 (the representative composite). The presence of



 

View Article Online
DOI: 10.1039/D6TA01685E

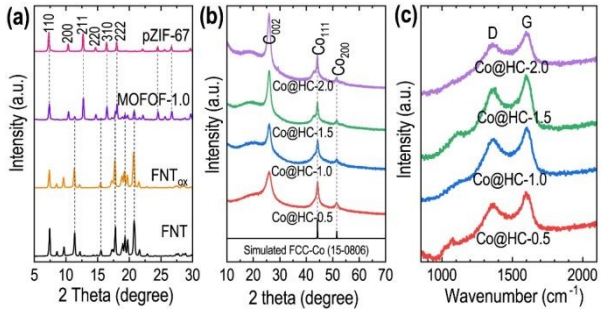


**Fig. 2**. (a) XRD patterns of FNT$_{ox}$, ZIF-67 and MOFOF-1.0; (b) XRD patterns of Co@HC-0.5, Co@HC-1.0, Co@HC-1.5, and Co@HC-2.0 materials and (c) Raman spectra of Co@HC-0.5, Co@HC-1.0, Co@HC-1.5, and Co@HC-2.0 materials.

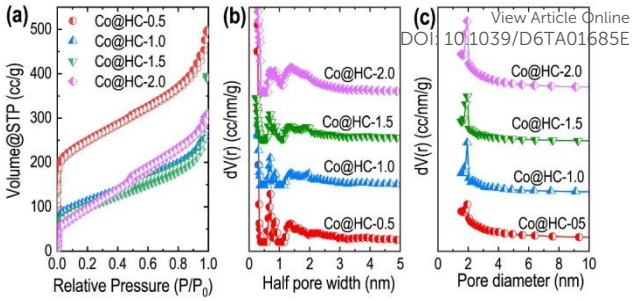


**Fig. 3**. (a) Nitrogen adsorption-desorption isotherms of Co@HC-0.5, Co@HC-1.0, Co@HC-1.5, and Co@HC-2.0 materials, (b) respective pore size distribution and the Barrett–Joyner–Halenda (BJH) model, and (c) corresponding pore size distribution profile obtained pore size distributions calculated using the DFT method.

characteristic ZIF-67 diffraction peaks in MOFOF-1.0 clearly confirms the successful integration of ZIF-67 onto FNT$_{ox}$, validating the formation of the composite nanostructures. Fig. 2b shows XRD patterns of the Co@HC-0.5, Co@HC-1.0, Co@HC-1.5, and Co@HC-2.0 materials, which obtained from the pristine MOFOF-0.5, MOFOF-1.0, MOFOF-1.5 and MOFOF-2.0, respectively. Moreover, Fig. S2 represents the XRD patterns of the FDC and Co@ZDC (i.e., carbonized FNT$_{ox}$ and pZIF-67, respectively). The XRD patterns in Fig. 2a and Fig. S2 are entirely different from those of the parent FNT$_{ox}$, pZIF-67, and MOFOF-1.0 composites (Fig. 2b). This indicates that the intrinsic peaks of the FNT$_{ox}$, pZIF-67, and MOFOF crystals disappeared and new peaks were observed concurrently, demonstrating the complete decomposition of FNT$_{ox}$, pZIF-67, and ZIF-67 crystalline phases in the MOFOF composites upon thermal and chemical treatment. The XRD patterns of Co@ZDC (Fig. S2), Co@HC-0.5, Co@HC-1.0, Co@HC-1.5, and Co@HC-2.0 (Fig. 2b) materials showed three new peaks at 26.0°, 44.2°, and 51.6°, which are the respective peaks for the 002 plane of graphitic carbon phase, 111 and 200 planes of the face-centered cubic (FCC) Co crystals.[47] The particle sizes of Co were estimated by using the Scherrer equation that revealed an increase with increasing the ZIF-67 content into the MOFOF precursors; for instance, the Co@HC-0.5, Co@HC-1.0, Co@HC-1.5, and Co@HC-2.0 materials had particle sizes of 3.3 nm, 5.8 nm, 7.3 nm, and 9.6 nm, respectively. The particle size of Co@ZDC was approximately 20 nm, significantly larger than that of Co@HCs.

As expected, the Co@HC materials obtained from the lowest ZIF-67 content have the smallest Co particles, which increase with increasing ZIF-67 content in the precursor MOFOF composite.

Fig. S2b and Fig. S2c depict the Raman spectra of the FDC, Co@ZDC, Co@HC-0.5, Co@HC-1.0, Co@HC-1.5, and Co@HC-2.0, where all the materials show two characteristic bands at 1353 cm$^{-1}$ and 1587 cm$^{-1}$, corresponding to the D-band and G-band with respect to the disordered sp$^3$ hybridized C atoms, and sp$^2$ hybridized graphitic C atoms, respectively.[48,49] The estimated intensity ratio ($I_D/I_G$) of the D and G bands (as shown in Fig. 2c) follows the order: FDC (1.05) < Co@HC-1.0 (1.32) < Co@HC-1.5 (1.37) < Co@HC-2.0 (1.42) < Co@ZDC (1.49). This trend indicates that higher ZIF-67 incorporation results in a greater degree of graphitization of the carbon phases. Here, the metallic cobalt in ZIF-67 enhances graphitization,[50,51] thereby increasing the $I_D/I_G$ ratio with higher ZIF-67 content in the precursor materials, consistent with the increased intensity of the C (002) peak in the XRD patterns (Fig. 2a).

Nitrogen sorption isotherms were recorded to determine the surface areas, pore volumes, and pore size distributions of the starting materials FNT$_{ox}$, pZIF-67, and MOFOFs (Fig. S3), and the resulting materials FDC, Co@ZDC, and Co@HCs after pyrolysis (Fig. S4 and Fig. 3). The isotherms are close to type I for MOFOFs, indicating primarily microporous structures, while

**Table 1**: Surface textural properties of FNT$_{OX}$, ZIF-67, MOFOFs and Co@HCs.

| Sample | $S_{BET}$ (m$^2$/g) | $S_{micro}$ (m$^2$/g) | $V_{micro}$ (cm$^3$/g) | $V_p$ (cm$^3$/g) | $D_p$ (nm) | $W_p$ (nm) |
|---|---|---|---|---|---|---|
| FNT$_{OX}$ | 36.9 | 18.0 | 0.050 | 0.118 | 1.63 | 1.38 |
| FDC | 530.17 | 461.2 | 0.338 | | 2.62 | |
| ZIF-67 | 744.7 | 614.9 | 0.423 | 0.535 | 1.54 | 0.54 |
| Co@ZDC | 194.9 | 136.4 | 0.267 | 0.511 | 1.95 | 0.57 |
| MOFOF-0.5 | 199.3 | 44.5 | 0.094 | 0.19 | 1.94 | 1.94 |
| Co@HC-0.5 | 810.3 | 711.7 | 0.687 | 1.129 | 1.94 | 0.29 |
| MOFOF-1.0 | 306.6 | 279.6 | 0.281 | 0.658 | 1.94 | 0.45 |
| Co@HC-1.0 | 418.7 | 367.2 | 0.380 | 0.705 | 1.94 | 0.29 |
| MOFOF-1.5 | 405.3 | 331.3 | 0.321 | 0.638 | 1.55 | 0.45 |
| Co@HC-1.5 | 381.4 | 347.9 | 0.390 | 0.685 | 1.95 | 0.29 |
| MOFOF-2.0 | 543.9 | 469.4 | 0.408 | 0.611 | 1.55 | 0.51 |
| Co@HC-2.0 | 367.7 | 266.8 | 0.323 | 0.608 | 1.45 | 0.25 |

$S_{BET}$ = BET surface area, $S_{micro}$ = micropore surface area, $V_{micro}$ = micropore volume, $V_p$ = total pore volume, $D_p$ = average pore diameter obtained from the BJH analysis, and $W_p$ = average half pore width obtained from the DFT model.

View Article Online
DOI: 10.1039/D6TA01685E

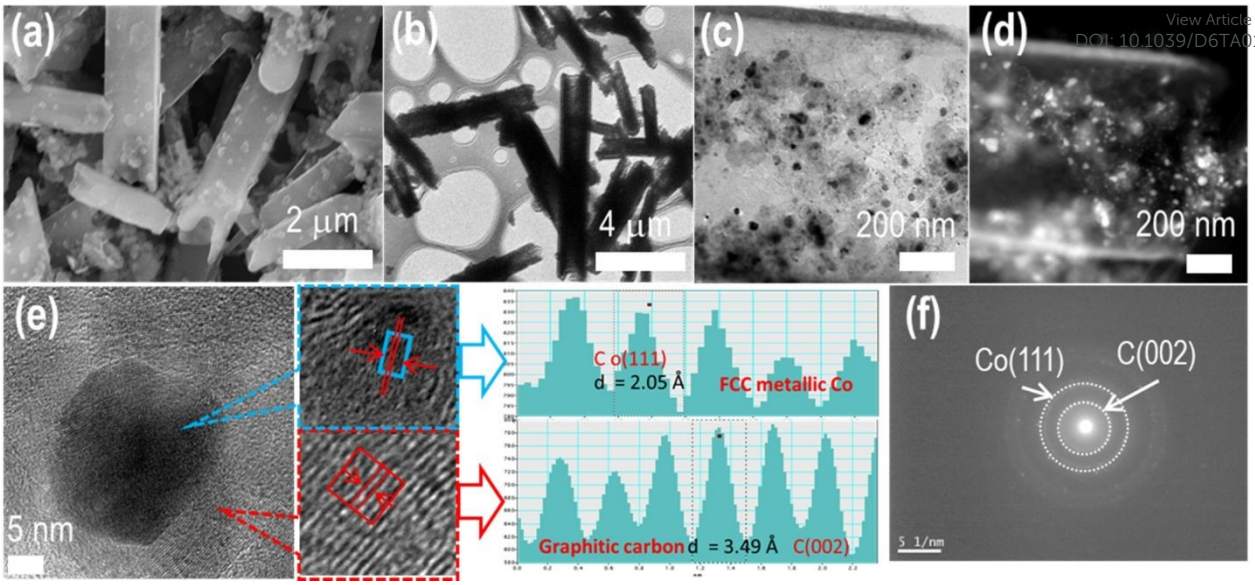


**Fig. 4**. (a) SEM image, (b) STEM image, (c) TEM image, (d) HAADF image, (e) HR-TEM image, lattice fringe and line-scanning intensity profile from the area highlighted regions and (f) SAED patterns of the Co@HC-1.0 materials.

$FNT_{ox}$ shows a type IV isotherm, indicating a nearly non-porous structure. Pore-size distribution analyses using the BJH (Fig. S3b) and DFT (Fig. S3c) methods, summarized in Table 1, indicated bimodal pore architectures in the composites. The isotherms for FDC, Co@ZDC, and Co@HCs exhibit Type-I/Type-IV mixed-type sorption (Fig. 3a), suggesting the formation of hierarchical micro- and mesoporous architectures. Large nitrogen adsorption at lower relative pressures ($P/P_0 < 0.05$) is attributed to micropore filling, while gradual nitrogen adsorption at higher pressures with a hysteresis loop is due to capillary condensation in mesopores.

Careful observation reveals that nitrogen adsorption at lower relative pressures decreases with increasing the $Co^{2+}/C_{60}$ ratio in the precursor MOFOFs, suggesting that mesoporosity development is influenced by the ZIF-67 content in the MOFOF composites during the carbonization. The pore-size distributions from the DFT method (Fig. 3b) and the BJH model (Fig. 3c) confirm the presence of both micropores and mesopores, indicating the hierarchical pore architecture of Co@HCs.

The surface textural parameters summarized in Table 1 show that the $Co^{2+}/C_{60}$ ratio in the precursor MOFOFs affects the surface area and porosity of the samples. The BET surface areas and pore volumes follow the order: FDC > Co@HC-0.5 > Co@HC-1.0 > Co@HC-1.5 > Co@HC-2.0 > Co@ZDC. The highest surface area in FDC is observed with complete carbonization of $FNT_{ox}$ in the absence of $Co^{2+}$ or ZIF-67, while Co@ZDC, derived from pZIF-67 with the highest Co content, shows the lowest surface area and pore volume. Additionally, the surface areas and pore volumes of Co@HC materials increase as the ZIF-67 content in the precursor MOF composites decreases, highlighting the influence of ZIF-67 or Co content on the porosity of Co@HCs. The hierarchical micro-/meso-pore architectures within Co@HC materials are advantageous for practical applications, particularly in heterogeneous catalysis.

Fig. 4 illustrates the SEM and TEM analyses of the representative Co@HC material, specifically Co@HC-1.0. The SEM and TEM images indicate that the morphology of MOFOF-1.0 remains unchanged after thermal and chemical treatment. Additionally, dark spots in the TEM image (Fig. 4c) and white spots in the HAADF image (Fig. 4d) confirm the uniform distribution of Co nanoparticles within the carbon nanocomposite. The interplanar d-spacing values, derived from the intensity profiles of the crystal lattice in the HR-TEM image (Fig. 4e), are 0.349 and 0.205 nm. These values closely match the d-spacings obtained from the SAED pattern (Fig. 4f), which are 0.346 nm and 0.205 nm, corresponding to the calculated d-spacings of 0.336 and 0.206 nm for the 002 plane of graphitic carbon[52] and the 111 plane of FCC Co crystals, respectively.[47,49] These findings confirm the formation of $sp^2$-hybridized graphitic carbon and FCC Co upon the thermal treatment of the MOFOF-1.0 composite, consistent with the XRD analysis (Fig. 1b).

Fig. 5 presents the X-ray photoelectron spectroscopy (XPS) analysis of MOFOF-1.0 (a representative MOFOF) and Co@HC-1.0 (a representative Co@HC) samples. The survey spectra (Fig. 5a) show the presence of carbon, oxygen, cobalt, and nitrogen in both materials. The atomic compositions observed are 78.3% C, 14.8% Co, 1.0% O, and 5.9% N for MOFOF-1.0, and 80.1% C, 1.5% Co, 16.2% O, and 2.2% N for Co@HC-1.0. The deconvoluted C 1s spectrum of MOFOF-1.0 (Fig. 5b) displays peaks at 284.1 eV (C=C, $sp^2$), 285.6 eV (C–C, $sp^3$/C–OH), and 286.4 eV (C–N). For Co@HC-1.0 (Fig. 5b), the C 1s spectrum reveals peaks at 284.3 eV (C–C), 285.6 eV (C–OH), 286.3 eV (C–O/C–N), and 288.7 eV (O–C=O). The O 1s spectra of both samples indicate similar C–OH and C–O–C bonding states with slight shifts (Fig. 5c). The deconvoluted N 1s spectrum of MOFOF-1.0 (Fig. 5d) shows peaks at 400.05 eV (N–H) and 401.0

View Article Online
DOI: 10.1039/D6TA01685E

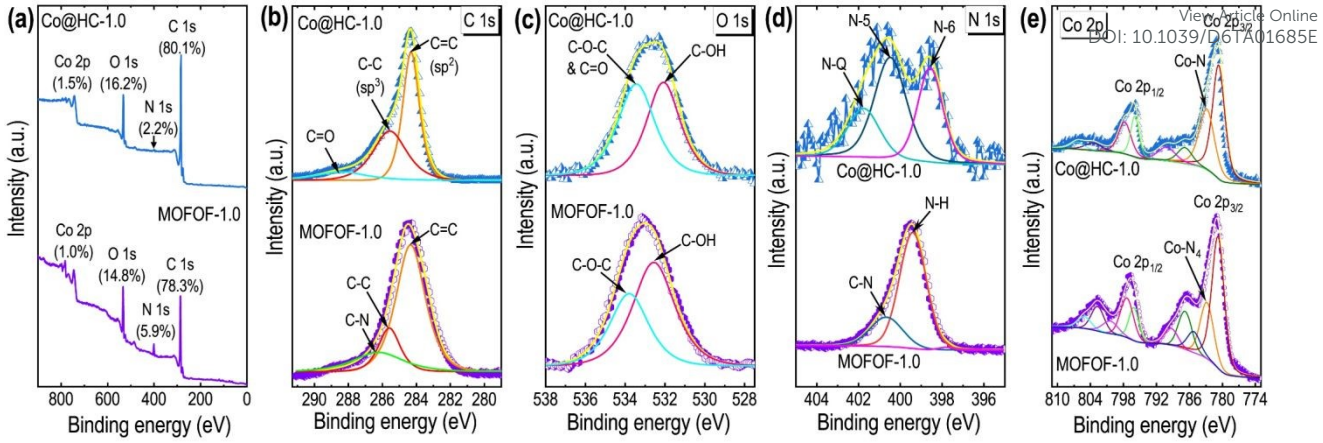


**Fig. 5**. (a) XPS observations of MOFOF-1.0 and Co@HC-1.0 materials. (a) XPS survey spectra, and deconvoluted (b) C 1s, (c) O 1s, (d) N 1s, and (e) Co 2p spectra.

eV (C–N), while for Co@HC-1.0 (Fig. 5d), the peaks correspond to pyridinic N (398.2 eV), pyrrolic N (400.2 eV), and quaternary N (401.4 eV).[53] The Co 2p spectrum of MOFOF-1.0 (Fig. 5e) shows a characteristic Co $2p_{3/2}$ peak at 781.1 eV accompanied by a satellite peak at 785.4 eV, which is attributed to $Co^{2+}$ species coordinated with nitrogen (Co–N), along with Co $2p_{1/2}$ peak at 796.2 with satellite peak at 802.64 eV, consistent with $Co^{2+}$ sites originating from the ZIF-67. In contrast, Co@HC-1.0 (Fig. 5e) features peaks at 780.35 eV and 795.95 eV assigned to the Co $2p_{3/2}$ and $2p_{1/2}$ levels of metallic $Co^0$, respectively.[54] Additionally, a peak at 782.4 eV indicates the presence of Co–N species, suggesting partial preservation of metal–nitrogen coordination after carbonization.

In summary, a MOFOF composite with different compositions was successfully developed via a simple, room-temperature in situ approach. The resulting MOFOF composites produced hierarchically porous carbon nanocomposites with well-dispersed Co nanoparticles supported on N-doped graphitic carbon. These small, well-distributed metallic Co nanoparticles, with Co–N bonding states on N-doped graphitic carbon supports, offer significant advantages for various catalytic reactions, including heterogeneous catalysis and electrochemical energy conversion.

### 3.2 Catalytic activities of the Co@HCs

The synthesized nanostructured hybrid carbons (Co@HCs) were utilized in the heterogeneous catalytic reduction of nitroarenes, addressing both environmental and chemical concerns. This reduction process is significant in organic synthesis due to the high value of the resulting aromatic amines or amino phenols.[55-60]

Fig. 6 shows the performance of the prepared FDC, Co@ZDC, and Co@HCs materials for catalytic reduction para nitrophenol (4-NP) in the presence of aqueous $NaBH_4$ under UV irradiation. Fig. 6a compares the effect of reaction time on the reduction of 4-NP over the FDC, Co@ZDC, and Co@HC catalysts, indicating that Co@HC-1.0 had the highest conversion efficiency, and FDC (without any Co-species) had the lowest conversion efficiency. Fig. 6b represents the pseudo-first-order kinetic plots over the tested catalysts, and the estimated kinetic parameters from the respective plots (Fig. 6b) are summarized in Table 2. The correlation coefficients ($R^2$) are very close to 1, which validates the successful use of the first-order kinetic model for the reduction of 4-NP over the studied catalysts. The estimated kinetic constants (k) confirm the highest reactivity of the Co@HC-1.0 for the reduction of 4-NP with an order of Co@HC-1.0 > Co@HC-1.5 > Co@ZDC > Co@HC-2.0 > FDC. The

**Table 2**: Pseudo-first-order rate constants and correlation coefficients of the reduction of nitroarene over Co@HC catalysts at room temperature.

| Materials | Co-content (atom%)[a] | Nitroarene substrate | Rate constant $K$ ($min^{-1}$) | Relative K[a] | $R^2$ | TOF ($h^{-1}$) |
|---|---|---|---|---|---|---|
| FDC | 0 | 4-NP | $6.4\times10^{-2}$ | 1 | 0.998 | – |
| Co@HC-0.5 | 1.2 | 4-NP | $1.63\times10^{-1}$ | 2.5 | 0.998 | 231 |
| Co@HC-1.0 | 1.5 | 4-NP | $9.25\times10^{-1}$ | 14.5 (1.3[b]) | 0.982 | 486 |
| Co@HC-1.5 | 2.3 | 4-NP | $4.16\times10^{-1}$ | 6.5 | 0.998 | 285 |
| Co@HC-2.0 | 3.1 | 4-NP | $3.09\times10^{-1}$ | 4.8 | 0.965 | 142 |
| Co@ZDC | 12.8 | 4-NP | $7.24\times10^{-1}$ | 11.3 | 0.997 | 55 |
| Co@HC-1.0 | 1.5 | 4Cl-NB | $3.5\times10^{-1}$ | – | 0.998 | – |
| Co@HC-1.0 | 1.5 | 2-NP | $3.5\times10^{-1}$ | – | 0.998 | – |
| Co@HC-1.0 | 1.5 | NB | $1.02\times10^{-1}$ | – | 0.990 | – |
| Co@HC-1.0 | 1.5 | 4Me-NM | $8.3\times10^{-1}$ | – | 0.995 | – |

[a]Co-content was analyzed by EDS analysis; [b]Relative k was estimated by considering the k of FDC as 1; [b]relative Co@ZDC

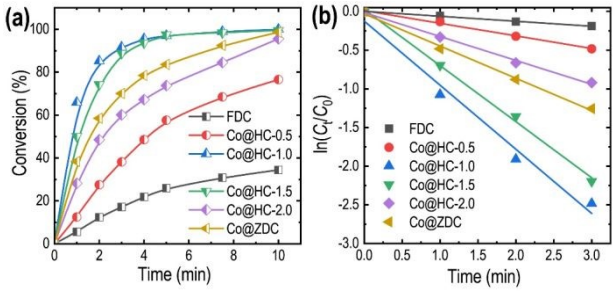


**Fig. 6**. (a) Effect of time and (b) plots of the pseudo-first-order kinetics for the reduction of 4-NP over the FDC, Co@HC-0.5, Co@HC-1.0, Co@HC-1.5, Co@HC-2.0, and Co-ZDC catalysts.

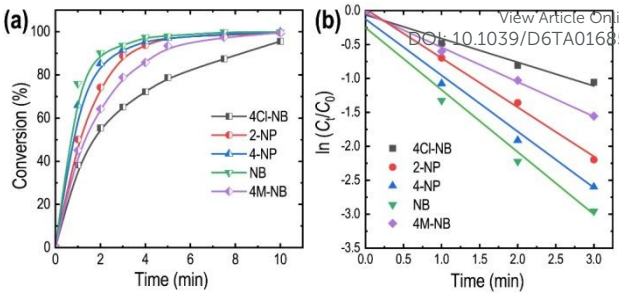


**Fig. 7**. (a) Effect of time and (b) plots of the pseudo-first-order kinetics for the reduction of different nitroarenes (i.e., 4Cl-NB, 2-NP, 4-NP, NB and 4M-NB) over the Co@HC-1.0 catalyst.

turnover frequency (TOF) values calculated from the 2-minute reaction data, summarized in Table 2, further demonstrate the superior performance of the Co@HC-1.0 catalyst. Consequently, Co@HC-1.0 stands out as a highly competitive catalyst among reported Co-based catalysts for the reduction of 4-NP, both in terms of the rate constant (k) and TOF, as detailed in the comparative analysis presented in Table S1.

Fig. 7 compares the reduction efficiencies of a series of nitroarenes with different or no substituents using the Co@HC-1.0 catalyst in the presence of $NaBH_4$. The effect of reaction time on nitroarene reduction (Fig. 7a) and the pseudo-first-order kinetic plots (Fig.7b) for the tested nitroarene reduction over the Co@HC-1.0 show different reactivity in terms of their conversion and kinetics (Table 2). The Co@HC-1.0 catalyst was, as expected, found to be very effective for the reduction of nitroarenes with different substituents, with reactivity varying among them.

The metal–N–carbon heterojunction in carbon materials, especially those with an enriched graphitic phase and doped with Co and N, can significantly enhance charge transfer, making them useful for various catalytic oxidation and reduction reactions.[51–63] Co and N-doped graphitic carbons with hierarchical porosity not only facilitate the adsorption of reactants but also ensure efficient mass transfer of reactants and intermediates/products. Additionally, doping with heteroatoms of different electronegativities (higher and lower) often produces a synergistic effect among the doped heteroatoms, driven by the unique electronic structure of these nanohybrid materials.[64,65] Therefore, the activity of the Co@HCs in nitroarene reduction reactions is likely governed by the Co–N coordination sites, Co nanoparticles, hierarchical porosity, N-doping, enriched graphitic carbon, and the synergistic effect between Co and N heteroatom.[66,67]

Both the Co–N coordination sites and Co nanoparticles, as evidenced by XPS, play a critical role in facilitating electron transfer from the reducing agent (here, $BH^{4-}$; the hydrogen donor) to the nitro group of nitroarenes. These sites act as catalytic centers, while graphitic carbon enhances electrical conductivity and electron mobility, and hierarchical porosity, and N-doping enhances mass transport, adsorption, and stability. Similar synergistic effects of Co–N–C systems have been widely reported in catalytic hydrogenation and electrochemical reactions.[59,60] The Co@HC-1.0 catalyst showed the highest catalytic activity for 4-NP reduction, despite having lower Co content (the main active sites) than Co@ZDC, Co@HC-1.5, and Co@HC-2.0, but slightly higher than Co@HC-0.5. Additionally, Co@HC-1.0 has higher surface area and pore volumes than Co@ZDC, Co@HC-1.5, and Co@HC-2.0, but lower than Co@HC-0.5. A detailed comparison of Table 1 and Table 2 reveals that Co@HC-1.0 achieves an optimal balance between Co content (1.5 at%), moderate particle size (~5.8 nm), and hierarchical porosity ($S_{BET}$ = 418.7 $m^2/g$). In contrast, Co@HC-0.5, despite a higher surface area, contains insufficient Co active sites, whereas Co@HC-1.5 and Co@HC-2.0 exhibit larger Co particles and reduced surface areas, leading to lower catalytic efficiency. This demonstrates that catalytic performance is governed by a delicate interplay between active site density, nanoparticle size, and pore accessibility. These results indicate that both the optimal Co content with controlled particle size and distribution and the porosity of the Co@HCs are essential for achieving high conversion, kinetic rate, and TOF values for 4-NP reduction, rather than a single parameter.

The observed reactivity order for the reduction of different nitroarenes (as illustrated in Scheme 1) is: nitrobenzene (NB) > para-nitrophenol (4-NP) > ortho-nitrophenol (2-NP) > para-methyl nitrobenzene (4Me-NB) > para-chloro nitrobenzene (4Cl-NB). NB is the easiest to reduce because it lacks substituents that affect the nitro group. 4-NP, despite having an electron-donating group, is still relatively easy to reduce due to the -OH group in the para position. The ortho -OH group in 2-nitrophenol introduces steric hindrance, making it harder to

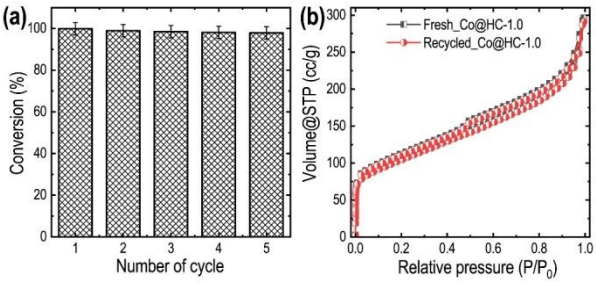


**Fig. 8**. (a) recyclability test results in terms of conversion of 4-NP over the Co@HC-1.0 catalyst; (b) Nitrogen adsorption-desorption isotherms of the fresh and recycled Co@HC-1.0 catalyst.

View Article Online
DOI: 10.1039/D6TA01985E

reduce. The methyl group in 4-methyl-nitrobenzene, being an electron-donating group, makes the nitro group less susceptible to reduction. Lastly, the chloro group in 4-chloro-nitrobenzene, due to its strong electron-withdrawing inductive effect, makes the nitro group the most electron-deficient and hardest to reduce.

### 3.3 Recyclability test

Fig. 8a illustrates the recyclability of the Co@HC-1.0 catalyst for the reduction of 4-NP. The results show only a slight decrease in reduction performance after five consecutive cycles. The catalyst was magnetically separated and regenerated by washing with ethanol and vacuum drying. Fig. 8b compares the $N_2$ adsorption-desorption isotherms of the fresh and recycled Co@HC-1.0 catalyst. The isotherms of the recycled catalyst (after four cycles) are very similar to those of the fresh catalyst, even after several uses, confirming the sustainability and recyclability of the developed catalyst. The negligible loss in catalytic activity, together with the nearly unchanged isotherms, suggests minimal Co leaching and excellent structural stability. No significant aggregation or loss of active sites was observed, although future ICP analysis could further quantify Co leaching. Overall, Co@HC-1.0 exhibits high catalytic activity, structural robustness, and excellent recyclability, making it a promising candidate for sustainable heterogeneous catalysis. Therefore, the precise nanoarchitectonics of Co-anchored, N-doped hierarchical carbon nanohybrids with controlled composition, distribution, and porosity effectively meet the requirements for a highly efficient and recyclable catalytic material, particularly for the reduction of nitroarenes.

## 4. Conclusions

In conclusion, we have successfully demonstrated the synthesis of hierarchical porous carbon nanostructures anchored with Co-metals by carbonizing newly developed MOFOF composites with well-distributed ZIF-67 on a self-assembled fullerene nanostructure. Unlike conventional ZIF-67-derived systems, the MOFOF approach incorporates fullerene nanotubes as a secondary carbon scaffold, creating a dual-carbon hierarchical framework that enhances Co dispersion, controls particle size, and strengthens interactions between Co, N-doped carbon, and graphitic domains, advantages not achievable in single-precursor MOF-derived materials. To the best of our knowledge, it is the first example of using a nanostructured MOFOF composite to get Co@HC materials. The Co@HCs possess a well-distribution of atomic level or ultrasmall Co-nanoparticles wrapped in a graphitic carbon layer on a hybrid carbon support with N-doping and hierarchical porosity and showed superior catalytic performance in the reduction of nitroarene compounds to the respective aromatic amines. The Co@HC-1.0 catalyst not only achieves high conversion efficiency in terms of kinetics and TOF values, but also superior reusability, and retains its structural integrity after multiple catalytic cycles. These findings indicate that Co@HC-1.0 is a highly effective and recyclable catalyst, with significant relevance to pharmaceutical synthesis and environmental remediation. Moreover, the hierarchical Co–N–C architecture exhibits strong potential for broader applications, including energy storage and electrocatalysis (e.g., ORR and $CO_2$ reduction), due to its high surface area, good conductivity, and tunable active sites. Overall, the successful nanoarchitecture of Co-anchored, N-doped hierarchical carbon nanohybrids with controlled composition and porosity offers a promising strategy for developing advanced catalytic materials.

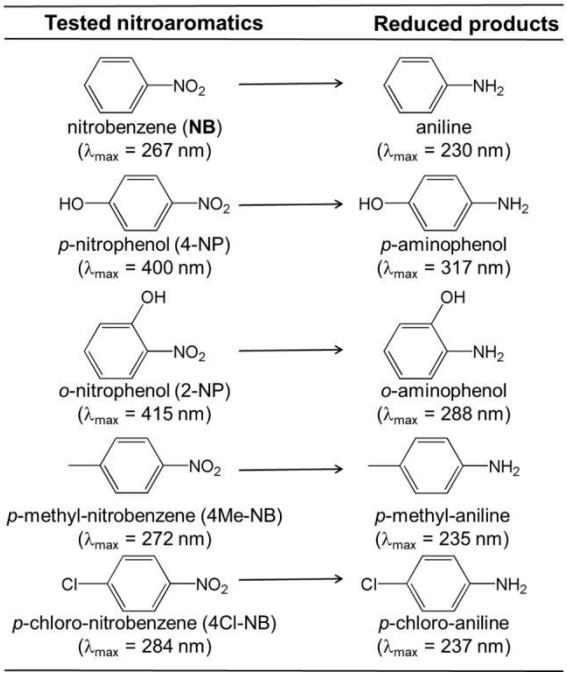


**Scheme 1**. Tested nitroarene substrates and their corresponding arylamine products obtained after reduction in aqueous medium using Co@HC-1.0 as the catalyst and $NaBH_4$ as the reducing agent. The corresponding UV–Vis absorption maxima ($\lambda_{max}$) of the nitroaromatic substrates and their reduced products in aqueous solution are also presented.

## Author contributions

B.N.B. and L.K.S. contributed equally to conceptualization and methodology. B.N.B., R.N.A., and S.S. contributed to the investigation. B.N.B., R.N.A., S.S., and L.K.S. contributed to data curation. B.N.B. and L.K.S. contributed to the preparation of the original draft. L.K.S. and K.A. contributed to the review and editing. L.K.S. and K.A. contributed to supervision and project administration. K.A. contributed to funding acquisition. All authors have read and agreed to the published version of the manuscript.

## Conflicts of interest

There are no conflicts to declare.

## Data availability

The data supporting this article have been included as part of the supplementary information (SI). Supplementary information is available.

## Acknowledgements

This study was partially supported by Japan Society for the Promotion of Science KAKENHI Grant Numbers, JP23H05459 and JP25H00898. R.N.A. and S.S. are thankful to the Ministry of Education, Culture, Sports, Science and Technology (MEXT) for the doctoral program scholarship.

## Notes and references

1 A. Pradhan and P. R. Gogate, *J. Hazard. Mater.*, 2010, **173**, 517–522. DOI: 10.1016/J.JHAZMAT.2009.08.115.
2 M. P. Rayaroth, C. T. Aravindakumar, N. S. Shah and G. Boczkaj, *Chem. Eng. J.*, 2022, **430**, 133002. DOI: 10.1016/J.CEJ.2021.133002.
3 M. I. Din, R. Khalid, Z. Hussain, T. Hussain, A. Mujahid, J. Najeeb and F. Izhar, *Crit. Rev. Anal. Chem.*, 2020, **50**, 322–338. DOI: 10.1080/10408347.2019.1637241.
4 M. Nasrollahzadeh, Z. Nezafat, M. G. Gorab and M. Sajjadi, Mol. Catal., 2020, **484**, 110758. DOI: 10.1016/J.MCAT.2019.110758.
5 D. Formenti, F. Ferretti, F. K. Scharnagl and M. Beller, *Chem. Rev.*, 2019, **119**, 2611–2680. DOI: 10.1021/acs.chemrev.8b00547.
6 C. Yao, W. Li, X. Ge, Y. Shi, Y. Cao, D. Chen, X. Zhou and X. Duan, *ChemCatChem*, 2024, **16**, e202400027. DOI: 10.1002/cctc.202400027.
7 J. Song, Z. F. Huang, L. Pan, K. Li, X. Zhang, L. Wang and J. J. Zou, *Appl. Catal. B, Environ.*, 2018, **227**, 386–408. DOI: 10.1016/J.APCATB.2018.01.052.
8 A. R. Patel, I. Patel and S. Banerjee, *Curr. Org. Chem.*, 2024, **28**, 375–389. DOI: 10.2174/0113852728296565240221082253.
9 H. Hu, J. H. Xin, H. Hu, X. Wang, D. Miao and Y. Liu, *J. Mater. Chem. A*, 2015, **3**, 11157–11182. DOI: 10.1039/C5TA00753D.
10 Q. Zhao, W. Ni, X. Tan, F. Cao, T. Liu, H. Huang, Z. Cheng, Y. Li, S. He, H. Ning and M. Wu, *J. Mater. Chem. A*, 2022, **10**, 9435–9444. DOI: 10.1039/D2TA00862A.
11 C. Huang, P. Qin, Y. Luo, Q. Ruan, L. Liu, Y. Wu, Q. Li, Y. Xu, R. Liu and P. K. Chu, *Mater. Today Energy*, 2022, **23**, 100911. DOI: 10.1016/J.MTENER.2021.100911.
12 M. Gäßler, J. Stahl, M. Schowalter, S. Pokhrel, A. Rosenauer, L. Mädler and R. Güttel, *ChemCatChem*, 2022, **14**, e202200286. DOI: 10.1002/CCTC.202200286.
13 C. Hernández Mejía, T. W. van Deelen and K. P. de Jong, *Nat. Commun.*, 2018, **9**, 1–8. DOI: 10.1038/s41467-018-06903-w.
14 M. Wolf, N. Fischer and M. Claeys, *Chem Catal.*, 2021, **1**, 1014–1041. DOI: 10.1016/J.CHECAT.2021.08.002.
15 H. Furukawa, K. E. Cordova, M. O'Keeffe and O. M. Yaghi, *Science*, 2013, **341**, 1230444. DOI:10.1126/SCIENCE.1230444.
16 D. Li, A. Yadav, H. Zhou, K. Roy, P. Thanasekaran and C. Lee, *Global Challenges*, 2024, **8**, 2300244. DOI: 10.1002/GCH2.202300244.
17 L. Shi, K. O. Kirlikovali, Z. Chen and O. K. Farha, *Chem*, 2024, **10**, 484–503. DOI: 10.1016/j.chempr.2023.09.005.
18 Q. L. Zhu and Q. Xu, *Chem. Soc. Rev.*, 2014, **43**, 5468–5512. DOI: 10.1039/C3CS60472A.
19 Y. Xue, S. Zheng, H. Xue and H. Pang, *J. Mater. Chem. A*, 2019, **7**, 7301–7327. DOI: 10.1039/C8TA12178H.
20 B. N. Bhadra and S. H. Jhung, *Chem. Eng. J.*, 2020, **398**, 125590. 10.1016/J.CEJ.2020.125590.
21 P. Huang, W. Wu, M. Li, Z. Li, L. Pan, T. Ahamad, S. M. Alshehri, Y. Bando, Y. Yamauchi and X. Xu, *Coord. Chem. Rev.*, 2024, **501**, 215534. DOI: 10.1016/j.ccr.2023.215534.
22 M. Kalaj, K. C. Bentz, S. Jr. Ayala, J. M. Palomba, K. S. Barcus, Y. Katayama and S. M. Cohen, *Chem. Rev.*, 2020, **120**, 8267–8302. DOI: 10.1021/acs.chemrev.9b00575.
23 X. W. Liu, T. J. Sun, J. L. Hu and S. D. Wang, *J. Mater. Chem. A*, 2016, **4**, 3584–3616. DOI: 10.1039/C5TA09924B.
24 A. Haruna, Z. U. Zango, G. Tanimu, T. Izuagie, S. G. Musa, Z. N. Garba, Z. M. A. Merican, *J. Environ. Chem. Eng.*, 2024, **12**, 113542. DOI: 10.1016/j.jece.2024.113542.
25 K. M. Z. Hasan, G. Lee, N. A. Khan, S. H. Jhung, *Coord. Chem. Rev.*, 2025, **534**, 216592. DOI: 10.1016/j.ccr.2025.216592.
26 W. Yang, X. Li, Y. Li, R. Zhu and H. Pang, *Adv. Mater.*, 2019, **31**, 1804740. DOI: 10.1002/adma.201804740.
27 K. Shen, X. Chen, J. Chen and Y. Li, *ACS Catal.*, 2016, **6**, 5887–5903. DOI: 10.1021/acscatal.6b01222.
28 C. Wang, J. Kim, J. Tang, M. Kim, H. Lim, V. Malgras, J. You, Q. Xu, J. Li and Y. Yamauchi, *Chem*, 2020, **6**, 19–40. DOI: 10.1016/J.CHEMPR.2019.09.005.
29 A. Han, B. Wang, A. Kumar, Y. Qin, J. Jin, X. Wang, C. Yang, B. Dong, Y. Jia, J. Liu and X. Sun, *Small Methods*, 2019, **3**, 1800471. DOI: 10.1002/SMTD.201800471.
30 H. F. Wang, L. Chen, H. Pang, S. Kaskel and Q. Xu, *Chem. Soc. Rev.*, 2020, **49**, 1414–1448. DOI: 10.1039/C9CS00906J.
31 B. N. Bhadra, A. Vinu, C. Serre and S. H. Jhung, *Mater. Today*, 2019, **25**, 88–111. DOI: 10.1016/J.MATTOD.2018.10.016.
32 D. Liu, W. Gu, L. Zhou, L. Wang, J. Zhang, Y. Liu and J. Lei, *Chem. Eng. J.*, 2022, **427**, 131503. DOI: 10.1016/J.CEJ.2021.131503.
33 C. Wang, Y. Yao, J. Li and Y. Yamauchi, *Acc. Mater. Res.*, 2022, **3**, 426–438. DOI: 10.1021/accountsmr.1c00258.
34 M. M. H. Mondol, I. Ahmed, H. J. Lee, A. Morsali, S. H. Jhung, Coord. Chem. Rev., 2023, **495**, 215382. DOI: 10.1016/j.ccr.2023.215382.
35 M. Liu, Q. Xu, Q. Miao, S. Yang, P. Wu, G. Liu, J. He, C. Yu, G. Zeng, *J. Mater. Chem. A*, 2022, **10**, 228-233. DOI: 10.1039/D1TA08325B.
36 M. Huang, L. Wang, K. Pei, W. You, X. Yu, Z. Wu and R. Che, *Small*, 2020, **16**, 2000158. DOI: 10.1002/smll.202000158.
37 X. Duan, N. Pan, C. Sun, K. Zhang, X. Zhu, M. Zhang, L. Song and H. Zheng, *J. Energy Chem.*, 2021, **56**, 290–298. DOI: 10.1016/J.JECHEM.2020.08.007.
38 H. D. Mai, P. M. Park, G. N. Bae, S. Jeong, B. Seo, M. Cho, S. Park, N. D. Cuong, T. V. Cuong, N. M. Tran, C. M. Park and K. J. Jeon, *J. Mater. Chem. A*, 2024, **12**, 4761–4769. DOI: 10.1039/D3TA07125A.
39 Y. Hu, C. Bai, M. Li, M. Hojamberdiev, D. Geng and X. Li, *J. Mater. Chem. A*, 2022, **10**, 3190–3200. DOI: 10.1039/D1TA09645A.
40 M. Huang, K. Mi, J. Zhang, H. Liu, T. Yu, A. Yuan, Q. Kong and S. Xiong, *J. Mater. Chem. A*, 2016, 5, 266–274. DOI: 10.1039/C6TA09030C.
41 B. N. Bhadra, L. K. Shrestha and K. Ariga, *CrystEngComm*, 2022, **24**, 6804–6824. DOI: 10.1039/D2CE00872F.
42 L. K. Shrestha, R. G. Shrestha, Y. Yamauchi, J. P. Hill, T. Nishimura, K. Miyazawa, T. Kawai, S. Okada, K. Wakabayashi and K. Ariga, *Angew. Chem. Int. Ed.*, 2015, **54**, 951–955. DOI: 10.1002/anie.201408856.
43 Q. Tang, P. Bairi, R. G. Shrestha, J. P. Hill, K. Ariga, H. Zeng, Q. Ji and L. K. Shrestha, *ACS Appl. Mater. Interfaces*, 2017, **9**, 44458–44465. DOI: 10.1021/acsami.7b13277.
44 Z. He, P. Wei, T. Xu, Z. Guo, J. Han, T. Akasaka, K. Guo and X. Lu, *Nanoscale*, 2022, **14**, 473–481. DOI: 10.1039/D1NR07198J.
45 Z. He, P. Wei, N. Chen, J. Han and X. Lu, *Chem. Eur. J.*, 2021, **27**, 1423–1429. DOI: 10.1002/CHEM.202004535.

View Article Online
DOI: 10.1039/D6TA01685E



46 A. V Baskar, M. R. Benzigar, S. N. Talapaneni, G. Singh, A. S. Karakoti, J. Yi, A. H. Al-Muhtaseb, K. Ariga, P. M. Ajayan and A. Vinu, *Adv. Funct. Mater.*, 2022, **32**, 2106924. DOI: 10.1002/adfm.202106924.
47 B. N. Bhadra, N. A. Khan and S. H. Jhung, *J. Mater. Chem. A*, 2019, **7**, 17823–17833. DOI: 10.1039/c9ta03613j.
48 M. Minakshi, A. Mujeeb, J. Whale, R. Evans, R. Aughterson, P. A. Shinde, K. Ariga and L. K. Shrestha, *Chempluschem*, 2024, **89**, e202400408. DOI: 10.1002/cplu.202400408.
49 B. N. Bhadra, M. M. H. Mondol and S. H. Jhung, *Sep. Purif. Technol.*, 2024, **330**, 125425. DOI: 10.1016/j.seppur.2023.125425.
50 M. Ranković, A. Janošević Ležaić, N. Gavrilov, I. Pašti, D. Bajuk-Bogdanović, B. N. Vasiljević, M. Savić, J. Krstić and G. Ćirić-Marjanović, *Mater. Chem. Phys.*, 2026, **348**, 131530. DOI: 10.1016/j.matchemphys.2025.131530.
51 A. Y. Maulana, S. Kim, J. H. Shim, C. Lee, J. Song, D. W. Lee, B. Yun, H. Gim, C. M. Futalan and J. Kim, *J. Alloys Compd.*, 2022, **908**, 164645. DOI: 10.1016/j.jallcom.2022.164645.
52 J. Tang, R. R. Salunkhe, H. Zhang, V. Malgras, T. Ahamad, S. M. Alshehri, N. Kobayashi, S. Tominaka, Y. Ide, J. H. Kim and Y. Yamauchi, *Sci. Rep.*, 2016, **6**, 30295. DOI: 10.1038/srep30295.
53 W. Orellana, C. Z. Loyola, J. F. Marco and F. Tasca, *Sci. Rep.*, 2022, **12**, 8072. DOI: 10.1038/s41598-022-11820-6.
54 B. Jiang, G. Zhang, Q. Tang, F. Meng, D. Zhou, W. Zhao, W. Jiang and Q. Ji, *Mater. Adv.*, 2022, **3**, 1539–1546. DOI: 10.1039/d1ma00937k.
55 J. Yao, L. Wang, D. Xie, L. Jiang, J. Li and X. Fang, *Front. Chem.*, 2022, **10**, 1000680. DOI: 10.3389/fchem.2022.1000680.
56 W. Guo, Y. Zheng, W. Xiang and Y. Zhang, *RSC Sustainability*, 2025, **3**, 243–254. DOI: 10.1039/d4su00531g.
57 L. Ruan, X. Han, L. Zhu, C. Shang, A. Kroner, K. Liu, Y. Zhang, B . H. Chen, Z. Guo, *Appl. Catal. B Environ.*, 2025, **379**, 125686. DOI: 10.1016/j.apcatb.2025.125686.
58 L. Zhu, H. Zhang, H. Zhu, H. Fu, A. Kroner, Z. Yang, H. Ye, B. H. Chen, R. Luque, *J. Catal.*, 2022, **413**, 978–991. DOI: 10.1016/j.jcat.2022.08.012.
59 K. Chen, Q. Liu, Z. Qiu, H. Zhang, N. Gonga, L. Zhu, *J. Mater. Chem. A*, 2024,**12**, 23940-23947. DOI: 10.1039/D4TA03635B.
60 Q. Liu, Y. Zhong, H. Fu, R. Wang, L. Zhu, *Appl. Catal. A: Gen.*, 2023, **665**, 119373. DOI: 10.1016/j.apcata.2023.119373.
61 X. Feng, Y. Bai, M. Liu, Y. Li, H. Yang, X. Wang and C. Wu, *Energy Environ. Sci.*, 2021, **14**, 2036–2089. DOI: 10.1039/D1EE00166C.
62 X. Li, C. Zeng, J. Jiang and L. Ai, *J. Mater. Chem. A*, 2016, **4**, 7476–7482. DOI: 10.1039/C6TA01054G.
63 H. Chen, K. Shen, Q. Mao, J. Chen and Y. Li, *ACS Catal.*, 2018, **8**, 1417–1426. DOI: 10.1021/acscatal.7b03270.
64 Y. Zheng, Y. Jiao, L. Ge, M. Jaroniec and S. Z. Qiao, *Angew. Chem. Int. Ed.*, 2013, **52**, 3110–3116. DOI: 10.1002/anie.201209548.
65 L. Zhang, M. Zhou, A. Wang and T. Zhang, *Chem. Rev.*, 2020, **120**, 683–733. DOI: 10.1021/acs.chemrev.9b00230.
66 D. T. Oyekunle, B. Wu, F. Luo, J. Ali and Z. Chen, *Chem. Eng. J.*, 2021, **421**, 129818. DOI: 10.1016/J.CEJ.2021.129818.
67 H. Chen, K. Shen, J. Chen, X. Chen and Y. Li, *J. Mater. Chem. A*, 2017, **5**, 9937–9945. DOI: 10.1039/C7TA02184D.